01 Jan 2000

Double-Slit Model for Partially Wetted Trickle Flow Hydrodynamics

I. Iliuta

F. Larachi

M. (Muthanna) H. Al-Dahhan
Missouri University of Science and Technology, aldahhanm@mst.edu

Recommended Citation

I. Iliuta et al., "Double-Slit Model for Partially Wetted Trickle Flow Hydrodynamics," *AIChE Journal*, vol. 46, no. 3, pp. 597 - 609, Wiley; American Institute of Chemical Engineers (AIChE), Jan 2000.
The definitive version is available at https://doi.org/10.1002/aic.690460318

Double-Slit Model for Partially Wetted Trickle Flow Hydrodynamics

I. Iliuta and F. Larachi
Dept. of Chemical Engineering & CERPIC, Laval University, Québec, P.Q., Canada G1K 7P4

M. H. Al-Dahhan
Chemical Reaction Engineering Laboratory, Chemical Engineering Dept., Washington University, St. Louis, MO 63130

A double-slit model developed can predict the frictional two-phase pressure drop, external liquid holdup, pellet-scale external wetting efficiency, and gas–liquid interfacial area in cocurrent downflow trickle-bed reactors operated under partially wetted conditions in the trickle flow regime. The model, an extension of the Holub et al. (1992, 1993) mechanistic pore-scale phenomenological approach, was designed to mimic the actual bed void by two inclined and interconnected slits: wet and dry slit. The external wetting efficiency is linked to both the pressure drop and external liquid holdup. The model also predicts gas–liquid interfacial areas in partially wetted conditions. An extensive trickle-flow regime database including over 1,200 measurements of two-phase pressure drop, liquid holdup, gas–liquid interfacial area and wetting efficiency, published in 1974–1998 on the partial-wetted conditions, was used to validate the modeling approach. Two new improved slip-factor functions were also developed using dimensional analysis and artificial neural networks. High-pressure and -temperature wetting efficiency, liquid holdup, pressure drop, and gas–liquid interfacial area data from the literature on the trickle-flow regime using conventional monosized beds and catalyst bed-dilution conditions were successfully forecasted by the model.

Introduction

Trickle-bed reactors (TBRs) have achieved widespread commercial acceptance in many gas–liquid–solid catalytic industrial applications. They are mainly employed in the petroleum (hydrocracking, hydrodesulfurization, hydrodenitrogenation, alkylation, etc.), petrochemical, and chemical industries (hydrogenation of higher aldehydes, reactive amination, liquid-phase oxidation, etc.), in the catalytic abatement of aqueous biocidal compounds, in bio- and electrochemical processing (Meyers, 1996; Dudukovic et al., 1999). The vast majority of industrial TBRs operates under extreme severity such as high pressure in order to handle large gas volumes, to enhance the gaseous reactant solubility in liquids to be processed, and to promote heat and mass transfers. Although TBRs can experience a variety of flow patterns, trickle-flow regime is of particular industrial interest. In this particular regime, the catalyst pellets can be either partially externally wetted at low liquid velocities or fully externally wetted at sufficiently high liquid velocities.

Holdup and pressure drop

A great many studies on trickle-flow regime carried out over the past few decades focused on liquid holdup and pressure-drop measurements in pilot and laboratory-scale TBRs. Liquid holdup is defined as the liquid-volume fraction per unit-reactor volume. It is indeed a basic parameter in reactor design owing to its relationship with other key hydrodynamic parameters such as pressure gradient, interfacial mass-transfer parameters, liquid mean residence time, catalyst loading-to-liquid volume ratio, liquid axial dispersion, radial effective thermal conductivity, and convective wall heat transfer coefficient. For highly exothermic reactions, the knowledge of this parameter is crucial for both circumventing hot-spot inception and preventing reactor runaway. Liquid holdup also affects catalyst external wetting efficiency, which in turn has an

Correspondence concerning this article should be addressed to F. Larachi.
Present address of I. Iliuta: Department of Chemical Engineering, Faculty of Industrial Chemistry, University Politehnica of Bucharest, Polizu 1, 78126 Bucharest, Romania.

impact on reaction selectivity, depending on whether a reaction is taking place solely on the wetted catalyst area or on dry and wetted areas alike.

The pressure drop represents the energy dissipated to offset the resistance to fluid motion through the reactor bed. It is important in determining energy losses, the sizing of the compression and pumping devices, and very often, in assessing the liquid holdup, the external wetting efficiency, the interfacial mass-transfer coefficients levels, among other aspects (Wammes et al., 1991a; Al-Dahhan, 1993; Latifi et al., 1999). The vast majority of approaches devoted to the prediction of liquid holdup and pressure gradient in trickle flow was entirely empirical and, as often shown in the literature, lacked generalization. Thus far, the Holub (1990) 1-D segregated two-fluid model and some twin models (''permeability'' model of Saez and Carbonell, 1985; CFD model of Attou et al., 1999), summarized in Table 1, have emerged as the best theoretical frameworks designed for the description of trickle-flow hydrodynamics. In the Holub (1990) model, the macroscopic unidirectional two-phase flow is mapped to a pellet-scale flow represented by a recurrent inclined slit. The gas flowing in the slit's central core is fully segregated from the liquid that flows as a thin film and fully wets the slit walls. The gas–liquid interface is considered impervious to momentum transfer (shearless boundary), and the interfacial gas velocity is assumed zero. Extension of the Holub shearless model to account for interfacial interactions between fluids via shear and velocity slip factors (f_s and f_v) was later attempted by Al-Dahhan et al. (1998) and Iliuta et al. (1998). Accordingly, the last authors derived generalized slip-factor functions using neural networks, dimensional analysis, and a wide-ranging trickle-flow database. In its last version, the extended Holub model significantly improved frictional pressure drop and liquid holdup predictions in trickle-flow regime, especially under fully wetted bed conditions (Iliuta et al., 1998). It is worth stating that no theoretical treatment of trickle-flow hydrodynamics under partial wetting conditions has, thus far, been attempted. Indeed, neither of the unidirectional models mentioned above (Holub, 1990; Saez and Carbonell, 1985; Attou et al., 1999) have addressed this aspect.

Wetted efficiency

Pellet-scale incomplete external wetting is the cause of deficient catalyst utilization. This in turn can lead to poor catalyst effectiveness factors and poor heat withdrawal from partially wetted catalyst pellets (Dudukovic and Mills, 1986;

Table 1. Recent Liquid Holdup, Pressure Drop, and Wetting Efficiency Models for Trickle-Flow Regime

Saez and Carbonell (1985)

$$\Psi_G = \frac{1}{(\epsilon - \epsilon_L)^{4.8}}\left[\frac{180\,Re_G}{Ga_G} + \frac{1.8\,Re_G^2}{Ga_G}\right] \tag{1}$$

$$\Psi_L = \left(\frac{\epsilon - \epsilon_L^s}{\epsilon_L - \epsilon_L^s}\right)^{2.43}\left[\frac{180\,Re_L}{Ga_L} + \frac{1.8\,Re_L^2}{Ga_L}\right] \tag{2}$$

Holub et al. (1992, 1993)

$$\Psi_G = \left(\frac{\epsilon}{\epsilon - \epsilon_L}\right)^3\left[\frac{E_1\,Re_G}{Ga_G} + \frac{E_2\,Re_G^2}{Ga_G}\right] \tag{3}$$

$$\Psi_L = \left(\frac{\epsilon}{\epsilon_L}\right)^3\left[\frac{E_1\,Re_L}{Ga_L} + \frac{E_2\,Re_L^2}{Ga_L}\right] \tag{4}$$

Holub et al. (1992) extended model modified by Al-Dahhan et al. (1998), Iliuta et al. (1998)

$$\Psi_G = \left(\frac{\epsilon}{\epsilon - \epsilon_L}\right)^3\left[\frac{E_1(Re_G - f_v(\epsilon - \epsilon_L)Re_i)}{Ga_G} + \frac{E_2(Re_G - f_v(\epsilon - \epsilon_L)Re_i)^2}{Ga_G}\right] \tag{5}$$

$$\Psi_L = \left(\frac{\epsilon}{\epsilon_L}\right)^3\left[\frac{E_1\,Re_L}{Ga_L} + \frac{E_2\,Re_L^2}{Ga_L}\right] + f_s\frac{(\epsilon - \epsilon_L)}{\epsilon_L}\left(1 - \frac{\rho_G}{\rho_L} - \Psi_L\right) \tag{6}$$

Attou et al. (1999)

$$\Psi_G = \left(\frac{1 - \epsilon + \epsilon_L}{1 - \epsilon}\right)^{2/3}\left\{\frac{180(1+\lambda)\,Re_G}{Ga_G}\left(\frac{\epsilon}{\epsilon - \epsilon_L}\right)^3\left(\frac{1 - \epsilon + \epsilon_L}{1 - \epsilon}\right)^2 + \frac{1.8(1+\lambda^2)\,Re_G^2}{Ga_G}\right\} \tag{7}$$

$$\Psi_L = -\frac{\epsilon - \epsilon_L}{\epsilon_L}\frac{\lambda\rho_G}{\rho_L}\left(\frac{1 - \epsilon + \epsilon_L}{1 - \epsilon}\right)^{2/3}\left\{\frac{180\,Re_G}{Ga_G}\left(\frac{\epsilon}{\epsilon - \epsilon_L}\right)^3\left(\frac{1 - \epsilon + \epsilon_L}{1 - \epsilon}\right)^2 + \frac{1.8\lambda\,Re_G^2}{Ga_G}\right\} + \frac{\epsilon^4}{(\epsilon - \epsilon_L)^3\epsilon_L}\left\{\frac{180\,Re_L}{Ga_L} + \frac{1.8\,Re_L^2}{Ga_L}\right\} \tag{8}$$

Pironti et al. (1999)

$$\eta_e = \frac{\beta_L(\rho_L - \rho_G) + \rho_L(\Psi_L - 1) - \rho_G\left(E_1\frac{Re_G}{Ga_G} + E_2\frac{Re_G^2}{Ga_G}\right)}{(\rho_L - \rho_G) + \left\{E_1\left(\rho_L\frac{Re_L}{Ga_L} - \rho_G\frac{Re_G}{Ga_G}\right) + E_2\left(\rho_L\frac{Re_L^2}{Ga_L} - \rho_G\frac{Re_G^2}{Ga_G}\right)\right\}}$$

McManus et al., 1993). Pellet-scale incomplete wetting arises when the tiny liquid irrigation rate feeding the bed is insufficient to ensure full coverage with a continuous liquid film of all pellets in the bed. Hence, the knowledge of the catalyst's external wetting efficiency as a function of operating conditions is needed to provide a relationship between laboratory and pilot-scale reactor data and the large-scale reactor operation for reliable scale-up/scale-down and design of commercial trickle-flow reactors. The reaction rate over externally incompletely wetted pellets can be greater or smaller than the rate observed over completely wetted ones. This depends upon whether the limiting reactant is present only in the liquid phase or in both fluids. If the reaction is liquid-limited and the liquid reactant is nonvolatile, then a decrease in the external wetting efficiency reduces the surface for liquid–solid mass transfer, thereby causing a decrease of the reaction rate. If the liquid reactant is volatile and heat effects are significant, then an additional reaction may also occur at the dry catalyst surface. Higher reaction rates can also be achieved through gas-limited reactions where the gaseous reactant can access the catalyst pores from the externally dry area. Therefore, in order to predict TBR performance and behavior, it is crucial to precisely quantify the catalyst external wetting efficiency and the effectiveness factor of the resulting partially wetted catalyst (Dudukovic, 1977; Mills and Dudukovic, 1981, 1982; Dudukovic and Mills, 1986; Zhukova et al., 1990). Several studies relative to the external wetting efficiency have been indeed reported in the literature (Shulman et al., 1955; Onda et al., 1967; Krauze and Serwinski, 1971; Puranik and Vogelpohl, 1974; Mills and Dudukovic, 1981; El-Hisnawi, 1981; Ruecker and Akgerman, 1987; Lazzaroni et al., 1988; Ring and Missen, 1991; Alicilar et al., 1994; Burghardt et al., 1995; Al-Dahhan and Dudukovic, 1995, 1996; Llano et al., 1997). Some deal with correlative and experimental methods of wetting efficiency, while others deal with demonstrating wetting effects on TBR reaction performance. Furthermore, the majority of wetting efficiency correlations were developed based on observations taken at ambient conditions (room temperature and barometric pressure). Very often, these conditions did not reveal any dependence of wetting efficiency upon gas throughput and density. Only Al-Dahhan and Dudukovic (1995, 1996) developed an empirical correlation between the wetting efficiency and the reactor pressure and the gas flow rates. Very recently, Pironti et al. (1999) proposed a macroscopic semitheoretical approach to predict total wetting efficiency. Although the approach is phenomenological, it requires the *a priori* measurements of liquid holdup, gas and liquid single-phase, and two-phase pressure gradients to compute the wetting efficiency. Thus far, the theoretical treatment of the coupling between the wetting efficiency and the trickle-flow hydrodynamic parameters remains elusive.

Gas–liquid interfacial area

In trickle-flow regime, gas–liquid mass-transfer resistances can be detrimental to the overall reactor performance, particularly at high pressure where the gas-side resistance is exacerbated by higher gas densities (Wammes et al., 1991a). Usually, gas–liquid mass transfer takes place across gas–liquid interfaces where the liquid can be stagnant or dynamic. While for slow reactions stagnant liquid affects the global reaction rate very little, fast reactions are characterized by a net contrast in reactant concentrations in the two regions, resulting in reactionally ineffective stagnant zones. When relatively fast reactions occur in the trickle-flow regime, the (effective) gas–liquid interfacial area is tantamount to the dynamic wetting efficiency. The two available correlations (Wild et al., 1992; Iliuta et al., 1999) relative to the prediction of the gas–liquid interfacial area validated over wide-ranging operating conditions are summarized in Table 2.

Table 2. Most Recent Gas–Liquid Interfacial Area Correlations for Trickle Flow

Wild et al. (1992)	
$\frac{a}{a_s} = 10\left[X_G\, Re_L^{-0.5} We_L \left(\frac{a_s d_h}{1-\epsilon} \right)^{1.5} \right]^{0.7}$	(10)
Iliuta et al. (1999)	
Neural network	
$ad_h/(1-\epsilon) = f(Re_L;\ Re_G;\ We_L;\ Fr_L;\ X_G;\ Eo_m;\ S_b)$	(11)

The objective of this contribution is to develop a two-fluid mechanistic model referred to as the ''double-slit model'' for the prediction of the frictional two-phase pressure drop, the liquid holdup, the gas–liquid interfacial area, the external wetting efficiency, and the partial-to-full wetting transition in the trickle-flow regime. The model is indeed a generalization of the Holub et al. (1992, 1993) phenomenological model, where partial wetting is incorporated to account for the shear stresses at both dry pellet–gas and gas–liquid interfaces. A comprehensive model validation has been performed using an extensive historic trickle-flow-regime database compiled from papers published from 1974 to 1998. This database includes more than 1200 measurements of the two-phase pressure drop, the liquid holdup, the gas–liquid interfacial area, and the wetting efficiency taken under partially wetted, high-pressure/temperature operation and catalyst bed dilution conditions.

Model Development

Pressure drop and liquid holdup model

At the pellet scale, the liquid texture in *trickle flow* can be decomposed into three components (Charpentier, 1968; Saez and Carbonell, 1985; Toye et al., 1997):

- Droplets;
- Quasi-stagnant liquid-film menisci at the pellets contact points;
- Pellet-supported wetting liquid films and rivulets.

The first texture component, that is, the droplets, is unlikely to occur in low-porosity beds and low liquid flow rates (Toye et al., 1997). The second component corresponds to the static liquid holdup and represents the liquid that remains entrapped in the bed after feed is cut off and the bed is drained. The third component is recognized as the dynamic liquid holdup. In the subsequent treatment, a general assumption is that both the second and the third liquid texture components, that is, total external liquid holdup, are embodied in one single structure referred to as ''liquid film.'' Thus as a result of small liquid irrigation rates and partial wetting, the liquid film carries, in a time-averaged sense, the totality

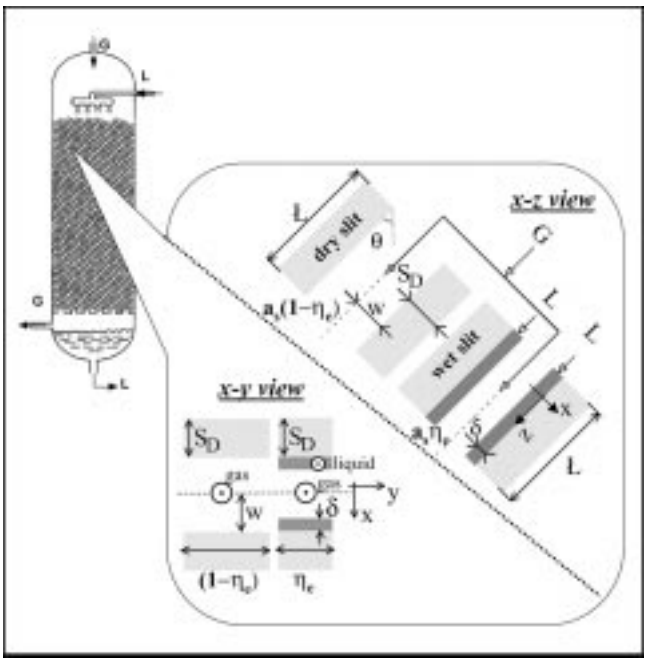

Figure 1. Double-slit model representation and two-phase flow distribution.

of the liquid flow rate in the form of a smooth and stable film.

The pressure drop and liquid holdup model is based on a representation of the actual void space at the pellet scale by a recurrent cell of two parallel interconnected inclined slits as shown in Figure 1. The first slit, corresponding to the region $a_s\eta_e$, is a wet slit moistened by the totality of the liquid flow rate in the form of a constant-thickness liquid film, while a fraction of the gas flows in the slit's central core. The second slit corresponding to the region $a_s(1-\eta_e)$ is a dry slit traversed exclusively by the remaining fraction of the gas flow rate. The geometrical features of the double-slit were mapped to those of the actual trickle bed by assuming:

- Identity of void-to-solid and liquid-to-solid volume ratios between slits and bed, that is

$$w/S_D = \epsilon/(1-\epsilon) \quad \text{and} \quad \delta\eta_e/S_D = \epsilon_L/(1-\epsilon)$$

- Equality of solid surface areas per unit solid volume in idealized slits and bed, that is, $S_D = d_p/6$
- Mapping of the average slit inclination (θ) to the bed tortuosity (T): $\cos\theta = 1/T$ (Holub, 1990), where T is the bed tortuosity defined as the ratio of actual flow path to the bed vertical height, and θ is the slit inclination (Figure 1)
- Split up of gas holdup in two components, that is, wet slit: $\epsilon\eta_e - \epsilon_L$ and dry slit: $\epsilon(1-\eta_e)$
- Equality of average velocities across the bed and representative slits, that is, $\langle u_{L,z}\rangle = v_{SL}T/\epsilon_L$ and $\langle u^{\text{wet}}_{G,z}\rangle = v_{SG}T\eta_e/(\epsilon\eta_e - \epsilon_L)$ for the wet slit, $\langle u^{\text{dry}}_{G,z}\rangle = v_{SG}T(1-\eta_e)/\epsilon(1-\eta_e) = v_{SG}T/\epsilon$ for the dry slit (index z stands for the streamwise flow in the pellet framework)
- To accommodate the various extents of wetting in the bed, the two slits possess equal streamwise lengths Ł ($x-z$ view of Figure 1) but different breadths ($x-y$ view of Figure 1): $(1-\eta_e)$ for the dry slit and η_e for the wet slit.

Further assumptions on the nature of the gas–liquid flow are:

- Steady-state and acceleration-free flow of liquid film (constant thickness) and gas
- Newtonian liquid
- Constant wall and gas–liquid interfacial shear stresses
- Interfacial friction factor, f_i, equal to wall friction factor, f_w
- Discontinuity in velocity and shear stress at gas–liquid interface: $u_{i,G} = f_v u_{i,L}$, $\tau_{i,L} = f_s\tau_{i,G}$.

With the preceding assumptions, the streamwise projections of the gas-phase momentum balance in the dry and wet slits become, respectively

$$(1-\eta_e)\tau_{w,G} = \left(-\frac{dP}{dz} + \rho_G g\cos\theta\right)w(1-\eta_e) \qquad (12)$$

$$\eta_e\tau_{i,G} = \left(-\frac{dP}{dz} + \rho_G g\cos\theta\right)(w-\delta)\eta_e. \qquad (13)$$

Combination of Eqs. 12 and 13 gives

$$-\frac{dP}{dz} + \rho_G g\cos\theta = \frac{\eta_e\tau_{i,G} + (1-\eta_e)\tau_{w,G}}{(w-\delta)\eta_e + w(1-\eta_e)}. \qquad (14)$$

Similarly, the streamwise projection of the momentum balance equation for the liquid phase in the wet slit is

$$-\frac{dP}{dz} + \rho_L g\cos\theta = \frac{\tau_{w,L} - \tau_{i,L}}{\delta}. \qquad (15)$$

In Eqs. 14 and 15, $\tau_{i,\alpha}$ represents the shear stress exerted on the α-phase side of the gas–liquid interface (wet slit), and $\tau_{w,\alpha}$ is the wall shear stress exerted by the wall on the α-phase (wet and dry slits). Furthermore, $\tau_{i,\alpha}$ and $\tau_{w,\alpha}$ possess laminar and turbulent contributions that can be computed by integrating the universal velocity profile within each fluid phase (Holub, 1990):

$$\tau_{i,G} = 2\frac{(u_G - u_{i,G})\mu_G}{w-\delta} + f_i\rho_G(u_G - u_{i,G})^2 \qquad (16)$$

$$\tau_{i,L} = f_s\tau_{i,G} \qquad (17)$$

$$\tau_{w,L} = 2\frac{u_L\mu_L}{\delta} + f_w\rho_L u_L^2 \qquad (18)$$

$$\tau_{w,G} = 2\frac{u_G\mu_G}{w} + f_w\rho_G u_G^2. \qquad (19)$$

With the aforementioned geometrical transformation relationships between the slits and the bed, Eqs. 14 and 15 are mapped from the slits scale to the bed scale leading to a two-fluid mechanistic model for trickle-bed hydrodynamics relating the pressure gradient, the liquid holdup, and the wetting efficiency. For the sake of conciseness, the lengthy derivation of this model is skipped and only the final form of the dimensionless model is summarized in Table 3 (Eqs. 20–28). Equations 20 and 21 are implicit algebraic equations with three unknowns, that is, $-\Delta P/H$, ϵ_L, η_e. For system

Table 3. Double-Slit Model

$$\Psi_L = \left(\frac{\epsilon}{\epsilon_L}\right)^3 \left[\eta_e^2 \frac{E_1 Re_L}{Ga_L} + \eta_e \frac{E_2 Re_L^2}{Ga_L}\right] + f_s\left(\frac{\eta_e \epsilon}{\epsilon_L} - 1\right)\left(1 - \frac{\rho_G}{\rho_L} - \Psi_L\right) \quad (20)$$

$$\Psi_G = \frac{\eta_e \epsilon^3}{\left(\epsilon - \frac{\epsilon_L}{\eta_e}\right)^2 (\epsilon - \epsilon_L)} \times \left\{ E_1 \frac{Re_G - f_v\left(\epsilon - \frac{\epsilon_L}{\eta_e}\right) Re_i}{Ga_G} + E_2 \frac{\left[Re_G - f_v\left(\epsilon - \frac{\epsilon_L}{\eta_e}\right) Re_i\right]^2}{Ga_G} \right\} + \frac{\epsilon(1-\eta_e)}{\epsilon - \epsilon_L}\left\{ E_1 \frac{Re_G}{Ga_G} + E_2 \frac{Re_G^2}{Ga_G} \right\} \quad (21)$$

$$\eta_e = \frac{\phi^2}{2E_1}\left(\frac{\epsilon_L}{\epsilon}\right)^2 \left(\Psi_L - 1 + \frac{\rho_G}{\rho_L}\right)\frac{Ga_L}{Re_L} f_s + \left\{ \left[\frac{\phi^2}{2E_1}\left(\frac{\epsilon_L}{\epsilon}\right)^2 \left(\Psi_L - 1 + \frac{\rho_G}{\rho_L}\right)\frac{Ga_L}{Re_L} f_s \right]^2 - \frac{\phi^2}{E_1}\left(\frac{\epsilon_L}{\epsilon}\right)^3 \left(\Psi_L - 1 + \frac{\rho_G}{\rho_L}\right)\frac{Ga_L}{Re_L} f_s + \frac{2\phi^2}{3E_1}\left(\frac{\epsilon_L}{\epsilon}\right)^3 \Psi_L \frac{Ga_L}{Re_L} \right\}^{1/2} \quad (38)$$

$$a = a_s \eta_e \left(1 - \frac{\epsilon_L^s}{\epsilon_L}\right) \quad (41)$$

$$\Psi_L = 1 + \frac{\rho_G}{\rho_L}(\Psi_G - 1) \quad (22)$$

$$Re_i = \frac{v_{iL} d_p}{\nu_L (1-\epsilon)} \quad (23)$$

$$Re_i = \Phi_L \eta_L \qquad 0 < \eta_L < 5 \quad (24)$$

$$Re_i = \Phi_L[-3.05 + 5\ln(\eta_L)] \qquad 5 < \eta_L < 30 \quad (25)$$

$$Re_i = \Phi_L[5.5 + 2.5\ln(\eta_L)] \qquad \eta_L > 30, \quad (26)$$

where

$$\Phi_L = \frac{10}{E_1^{3/4}} \frac{\nu_L}{\nu_G} \sqrt{\Psi_L Ga_L \frac{\epsilon_L}{\eta_e \epsilon^3}\left(1 + f_s \frac{\rho_G}{\rho_L}\frac{\Psi_G}{\Psi_L}\left(\frac{\eta_e \epsilon}{\epsilon_L} - 1\right)\right)} \quad (27)$$

$$\eta_L = \frac{1}{5E_1^{1/4}} \sqrt{\Psi_L Ga_L \left(\frac{\epsilon_L}{\epsilon \eta_e}\right)^3 \left(1 + f_s \frac{\rho_G}{\rho_L}\frac{\Psi_G}{\Psi_L}\left(\frac{\eta_e \epsilon}{\epsilon_L} - 1\right)\right)} \quad (28)$$

closure, an additional equation is required for the wetting efficiency, which is the purpose of the next section. It is instructive to note that with $\eta_e = 1$, Eqs. 20–28 degenerate to the expected extended Holub model (Table 1).

External wetting efficiency and gas–liquid interfacial-area model

The relationship between the wetting efficiency, the total liquid holdup, and the film thickness for partially wetted trickle flow conditions is

$$\epsilon_L = a_s \eta_e \delta. \quad (29)$$

The just mentioned assumption of equality of liquid film average velocities across the bed and the wet slit gives

$$\langle u_{L,z} \rangle = \frac{T v_{SL}}{\eta_e a_s \delta}. \quad (30)$$

A z-momentum balance over a liquid film of cross-stream thickness Δx (Figure 1) bounded by planes z and $z + \Delta z$ in the wet slit gives

$$\frac{d^2 u_{L,z}}{dx^2} = -\frac{\rho_L}{\mu_L} g \cos\theta + \frac{1}{\mu_L}\frac{dP}{dz} \quad (31)$$

subject to the boundary conditions

$$@\ x = 0: \ \frac{du_{L,z}}{dx} = \left(-\frac{\rho_G}{\mu_L} g \cos\theta + \frac{1}{\mu_L}\frac{dP}{dz}\right) f_s (w - \delta) \quad (32)$$

$$@\ x = \delta: \ u_{L,z} = 0. \quad (33)$$

Double integration of ODE Eq. 31 leads to the velocity distribution of the liquid film in the wet slit

$$u_{L,z} = \left(\rho_L g \cos\theta - \frac{dP}{dz}\right)\frac{\delta^2}{2\mu_L}\left[1 - \left(\frac{x}{\delta}\right)^2\right] + \left(\rho_G g \cos\theta - \frac{dP}{dz}\right)\frac{(w-\delta)\delta f_s}{\mu_L}\left(1 - \frac{x}{\delta}\right). \quad (34)$$

The liquid-film average velocity then becomes

$$\langle u_{L,z} \rangle = \frac{1}{\delta}\int_0^\delta u_{L,z}\, dx = \left(\rho_L g \cos\theta - \frac{dP}{dz}\right)\frac{\delta^2}{3\mu_L} + \left(\rho_G g \cos\theta - \frac{dP}{dz}\right)\frac{(w-\delta)\delta f_s}{2\mu_L}. \quad (35)$$

Combination of Eq. 30 with Eq. 35 provides the third implicit equation for closure of the hydrodynamic model

$$\frac{v_{SL}}{\eta_e a_s} = \left(\rho_L g \cos\theta - \frac{dP}{dz}\right)\frac{\delta^3 \cos\theta}{3\mu_L} + \left(\rho_G g \cos\theta - \frac{dP}{dz}\right)\frac{(w-\delta)\delta^2 f_s \cos\theta}{2\mu_L} = \Psi_L \rho_L g \frac{\left(\frac{\epsilon_L}{a_s \eta_e}\right)^3 \cos^2\theta}{3\mu_L} + \Psi_G \rho_G g \frac{\left(\frac{\epsilon}{a_s} - \frac{\epsilon_L}{a_s \eta_e}\right)^2 \left(\frac{\epsilon_L}{a_s \eta_e}\right)^2 f_s \cos^2\theta}{2\mu_L}, \quad (36)$$

where the total pressure gradient is the same for both the bed and the representative slits

$$\Psi_\alpha \rho_\alpha g = -\Delta P/H + \rho_\alpha g = -\frac{dP}{dz}\cos^{-1}\theta + \rho_\alpha g. \quad (37)$$

After manipulation of Eq. 36, the final dimensionless expression of the wetting efficiency in terms of the trickle-bed variables is given in Table 3 (Eq. 38).

Similar to the liquid holdup, the wetting efficiency can be split into two components, namely the static, η_e^s, and the dynamic, η_e^d, wetting efficiencies. Assuming, as a first approximation, a correspondence between the ratios of static-to-dynamic liquid holdup and static-to-dynamic wetting efficiency (Rajashekharam et al., 1998), then

$$\frac{\eta_e^d}{\eta_e^s} = \frac{\epsilon_L^d}{\epsilon_L^s} = \frac{\eta_e^d}{\eta_e - \eta_e^d} = \frac{\epsilon_L - \epsilon_L^s}{\epsilon_L^s}. \tag{39}$$

After rearrangement, the dynamic wetting efficiency is expressed as a function of the external and the static liquid holdups and the total wetting efficiency

$$\eta_e^d = \eta_e(1 - \epsilon_L^s/\epsilon_L). \tag{40}$$

As stipulated earlier, in the trickle-flow regime at small liquid irrigation rates, the contribution of the liquid film is likely to outweigh the droplet contribution. Furthermore, a smooth gas–liquid interface is expected from the tiny liquid-film thickness. In the circumstances of fast chemical reactions, the gas–liquid interfacial area becomes tantamount to the liquid–solid area wetted by the ''active'' dynamic liquid solely (Eq. 41, Table 3).

Results and Discussion

Comprehensive database

Wide-ranging databases are a prerequisite to any meaningful and useful model development for a highly accurate prediction of trickle-flow characteristics. Taking advantage of abundant experimental information related to the TBR open literature published worldwide between 1974 and 1998, a comprehensive database including liquid holdup, frictional pressure drop, gas–liquid interfacial area, and wetting efficiency for the trickle-flow regime under partially wetted conditions, and Ergun single-phase flow parameters was elaborated. A series of criteria formulated below have been identified to provide a procedure for selection and normalization of experimental data destined to be included in the database. Each criterion accents key characteristics, which a measurement datum must possess to meet the modeling application objectives of reliability and accuracy.

Criterion 1. Only measurements carried out far and down of the trickle-to-pulse flow regime boundary were selected. An objective criterion of a liquid superficial velocity at most fifth the liquid transition velocity was chosen.

Criterion 2. Liquid holdup was transformed into total external liquid holdup. Available dynamic holdups were summed up with external static holdups. For porous particles, total liquid holdups were transformed into external holdups by resting the intraparticle contribution.

Criterion 3. The total pressure gradient was converted into a frictional pressure gradient. The pressure variations occasioned in trickle flow by acceleration/deceleration were marginal, as verified by the Brunazzi and Paglianti (1997) relationship, and only the gravitational term was accounted for.

Key information on the database (1,200 experiments, 31 references) is summarized in Table 4. The hydrodynamic measurements were taken using 18 different liquids, pure and mixed, aqueous and organic, coalescing and noncoalescing; 5

Table 4. Description of Database

Fluid Physical Properties	Operating Conditions and Trickle-Flow Parameters	Limits of Dimensionless Groups
$780 \le \rho_L \le 1107$	$2.2\times10^{-4} \le v_{SL} \le 5.0\times10^{-3}$	$-8.5 \le f_s \le -8.3\times10^{-4}$
$6.32\times10^{-4} \le \mu_L \le 1.9\times10^{-2}$	$2.4\times10^{-3} \le v_{SG} \le 1.13$	$-135.6 \le f_v \le 0$
$1.06\times10^{-2} \le \sigma_L \le 7.5\times10^{-2}$	$0.1 \le P \le 10$ MPa	$1.50\times10^{-2} \le Re_L \le 91$
$0.16 \le \rho_G \le 58.0$	$13 \le T \le 350$°C	$1.9\times10^{-1} \le Re_G \le 471$
$1.66\times10^{-5} \le \mu_G \le 2.6\times10^{-5}$	$0.051 \le \epsilon_L \le 0.35$	$8.2\times10^{-8} \le Fr_L \le 4.2\times10^{-3}$
	$13.2 \le \Delta P/H \le 1\times10^5$	$1\times10^{-7} \le We_L \le 1.3\times10^{-2}$
	$0.2 \le \eta_e \le 1.0$	$6.9\times10^{-3} \le X_L \le 1.4\times10^2$
	$37.7 \le a \le 1430$	$4.6\times10^{-7} \le St_L \le 2.6\times10^{-3}$
Geometrical Properties of Packings and Columns		
Particle diameter, d_p (m)	$1.2\times10^{-3} \le d_p \le 2.54\times10^{-2}$	
Column diameter, d_c (m)	$2.3\times10^{-2} \le d_c \le 0.3$	
Bed porosity, ϵ	$0.30 \le \epsilon \le 0.94$	
Shape factor, ϕ	$0.133 \le \phi \le 1.0$	
Ergun constants	$65 \le E_1 \le 380$; $0.8 \le E_2 \le 3.1$	
Particle shape	sphere, cylinder, extrudate, Raschig, Pall ring, Intalox, Berl saddle	
Liquids: H_2O, H_2O + 1%EtOH, H_2O + NaOH [0.1–2.4 N], $H_2O + Na_2S_2O_3$, H_2O + DIPA* [1.8 M], $H_2O + Na_2SO_3$ [0.8 M], $H_2O + Na_2SO_4$ [1 M], H_2O + NaOH [0.5–2 N] + Na_2SO_4, MeOH, C_6H_{12}, EtOH + DEA* (0.645 M), EtOH + MEA* (0.183 M), ETG*, ETG* + MEA (1.43 M), H_2O + DEA [1.5–2 M], toluene + CHA* + 10% IPA*, toluene + 10% IPA + DIPA, DMA, H_2O + DEA [1.5 M] + ETG [20–40%], C_6H_{14}, desulfurized gas oil, kerosene		
Gases: Air, carbon dioxide + air, sulfur dioxide + air, nitrogen, air + oxygen, $N_2 + CO_2$		
Bibliographical Sources: Al-Dahhan (1993), Al-Dahhan and Dudukovic (1995, 1996), Azzaz (1984), Bakos et al. (1980), Fukushima and Kusaka (1977a,b), Iliuta (1996), Iliuta et al. (1996), Lakota (1990), Lakota and Levec (1990), Larachi (1991), Larachi et al. (1991a,b, 1992, 1997, 1998), Mahajani and Sharma (1979, 1980), Morsi (1982), Morsi et al. (1978, 1982, 1984), Ratnam et al. (1994), Shende and Sharma (1974), Yaïci (1985), Yaïci et al. (1985, 1988), Wammes (1990), Wammes et al. (1991a,b), Ring and Missen (1991), Llano et al. (1997).		

*CHA = cyclohexylamine; DEA = diethanolamine; DIPA = diisopropropanolamine; DMA = dimethylamine; ETG = ethylene glycol; IPA = isopropanolamine; MEA = monoethanolamine.

gases up to 10 MPa, columns of 9 different sizes packed with 15 packing materials. Furthermore, the interfacial area measurements were taken using 12 gas–liquid couples, more than 20 packing sizes and shapes, and 10 column sizes up to 5.0 MPa. The data relative to the wetting efficiency were selected from measurements carried out on nondiluted beds and diluted beds with fines up to 10 MPa and 623 K using spherical and nonspherical pellets. The database was arranged in matrix form. For the ease of cross-correlation calculations, each row contains the liquid and gas superficial velocities, the liquid and gas densities, the liquid and gas dynamic viscosities, the surface tension, the bed porosity, the particle equivalent diameter, the sphericity, the column diameter, the external liquid holdup, the frictional pressure drop, the gas–liquid interfacial area, and the wetting efficiency.

Estimation of slip factors

Solving the *direct problem* given by the model Eqs. 20–28, 38, and 41 (Table 3) requires that the Ergun constants, E_1 and E_2, the static liquid holdup, ϵ_L^s, and the slip factors, f_v and f_s, be *a priori* known to predict the frictional pressure drop, the total external liquid holdup, the wetting efficiency, and the gas–liquid interfacial area. The Ergun single-phase flow parameters and the static liquid holdup can be set either by measurements or estimated from the correlations (Saez and Carbonell, 1985; Iliuta et al., 1998). Unfortunately there exists no independent theoretical or experimental means giving access to the f_s and f_v slip factors. The only reliable f_v and f_s functions were set empirically, assuming full wetting of the bed (Iliuta et al., 1998). This approach is not valid for partially wetted beds, and hence requires the need to reevaluate the f_s and f_v slip factors. To bypass this lack of knowledge, (pseudo) experimental slip factor values were generated by solving, for each row of the database, the *inverse problem* given by the model Eqs. 20–28 and 38. This was performed by feeding this model with actual experimental data relative to the pressure drop and the liquid holdup and solving it for the unknowns, f_s and f_v. In the case of f_v, only the solution that fulfilled Prandtl's mixing length turbulence model is retained. The slip factors thus determined were correlated to the operating trickle-bed variables via combined dimensional analysis and three-layer perceptron artificial neural networks (ANNs).

As a result, a force analysis was indeed performed to identify the most meaningful forces exhibiting the highest cross-correlation coefficients with the slip factors. Phenomenologically such forces must scale with

- Inertia of liquid and gas, $F_{iL} = \rho_L v_{SL}^2$ and $F_{iG} = \rho_G v_{SG}^2$
- Liquid and gas viscous forces, $F_{vL} = \mu_L v_{SL}/d_p$ and $F_{vG} = \mu_G v_{SG}/d_p$
- Liquid gravitational force, $F_{gL} = \rho_L g d_p$
- Capillary force, $F_{cL} = \sigma_L/d_p$
- Gravitational force due to gas is likely marginal in the trickle-flow regime.

The most dominant forces being established, dimensional-statistical analysis was used to search for the best selection of dimensionless groups to express the slip factors (ANN outputs). Using more than 1,500 ANN architectures, over 100 combination sets were tested by trial and error until the most expressive set of dimensionless groups (ANN input vector) was extracted. This set corresponds to the following assortment of groups: Re_L, Re_G, Fr_L, We_L, liquid-to-gas inertia forces ratio (X_L), and liquid viscosity-to-gravity forces ratio or Stokes group (St_L).

Table 5. Set of Equations for Neural Network Correlations for Shear and Velocity Slip Factors

$$S_k = \frac{1}{1+\exp\left[-\sum_{j=1}^{J+1}\omega_{jk}H_{jk}\right]} \quad \text{for} \quad 1 \le k \le K \tag{42}$$

$$H_{jk} = \frac{1}{1+\exp\left[-\sum_{i=1}^{I+1}\omega_{ijk}U_i\right]} \quad \text{for} \quad 1 \le j \le J \tag{43}$$

f_s ($I = 6$, $J = 6$, $K = 1$) and f_v ($I = 6$, $J = 7$, $K = 2$)

$$S_1 = \frac{f_s + 7.46234}{7.4615} \qquad S_2 = \frac{f_v + 133.4493}{133.4357}$$

$$U_1 = \frac{\log\left(\frac{Re_L}{1.507\times10^{-2}}\right)}{3.781} \qquad U_2 = \frac{\log\left(\frac{Re_G}{1.944\times10^{-1}}\right)}{3.3843}$$

$$U_3 = \frac{\log\left(\frac{Fr_L}{8.166\times10^{-8}}\right)}{4.706} \qquad U_4 = \frac{\log\left(\frac{We_L}{1.0\times10^{-7}}\right)}{5.098}$$

$$U_5 = \frac{\log\left(\frac{X_L}{6.855\times10^{-3}}\right)}{4.320} \qquad U_6 = \frac{\log\left(\frac{St_L}{4.592\times10^{-7}}\right)}{3.755} \qquad U_7 = 1$$

The ANN architectures were designed using the NNFit software package (Cloutier et al., 1996). Based on the generic sigmoid-type stimulus given by Eqs. 42 and 43 (see Table 5), the neural network structures used to extract f_s and f_v are shown in Figure 2. The normalized f_s (or f_v) outputs, S_k, were correlated to the set of normalized input vector (Table 5) through a training procedure designed to configure the

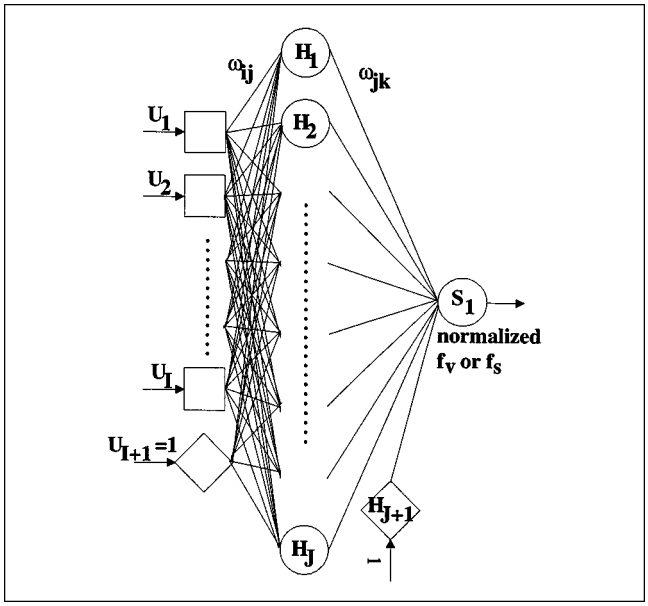

Figure 2. Architecture of the three-layer artificial-neural-network dimensionless correlations for shear and velocity slip factors.

Table 6. Fitting Parameters of the Neural Network Correlation for the Shear Slip Factor, f_s ($I = 6$, $J = 6$)

ω_{ij1}	1	2	3	4	5	6
1	−1.6191	0.3136	−1.0667	−1.7192	1.6136	−4.9765
2	10.4854	16.2984	13.0344	15.2944	7.1119	9.6108
3	0.9044	−0.8855	0.1516	−0.6282	1.8423	5.4631
4	−1.3005	1.2435	−1.8178	1.3543	−0.6845	−4.3849
5	−2.6925	−6.4154	−12.8196	−17.2175	−12.1212	−3.8823
6	3.0109	−4.3859	0.4482	2.4012	1.3807	8.4894
7	−1.2757	−6.8271	−2.5247	1.9412	1.9594	−4.1040

ω_{j1}	1	2	3	4	5	6	7
	−7.4202	3.5749	−2.1969	−4.6039	7.0897	4.1495	2.7124

ANN. The basic idea behind this learning operation consists of feeding the ANN input data patterns so as to produce associated output data patterns that closely match the desired or target output data. The approach amounts to finding a set of connectivity weights, ω_{jk} and ω_{ijk}, that minimizes, through the least-squares method, a cumulative error between the ANN output data and the desired data. The input/output data were indeed randomly selected to represent 70% of the total compiled experimental data contained in the database.

One good measure of performance of the trained network is known as generalization ability. It consists of investigating how closely the actual output of the neural network approximates the desired output data for an input (that is, the 30% remaining data) that has never been presented as learning patterns.

For each of f_s and f_v ANN, the number of hidden neurons, J, was varied from 3 to 15. Hidden layers with 6 neurons (for f_s) and 7 neurons (for f_v) were the optimal ANN architectures leading to the smallest average absolute relative errors (AAREs) on the training (8.3% for f_s and 12.8% for f_v) and the generalization sets (6.6% for f_s and 12.4% for f_v). The connectivity weights of the two ANNs are listed in Tables 6 and 7. The complete f_s, f_v ANN correlations are also available on the Net and accessible at the Web address: http://www.gch.ulaval.ca/~flarachi.

Pressure drop and liquid holdup

The model inputs consist of the fluid velocities and physical properties, the bed characteristics, and the operating conditions. These parameters enabled the evaluation of E_1, E_2, ϵ_L^s, f_v, and f_s. Furthermore, the double-slit model was solved iteratively by the Newton-Raphson method to predict the pressure drop, the liquid holdup, and the wetting efficiency.

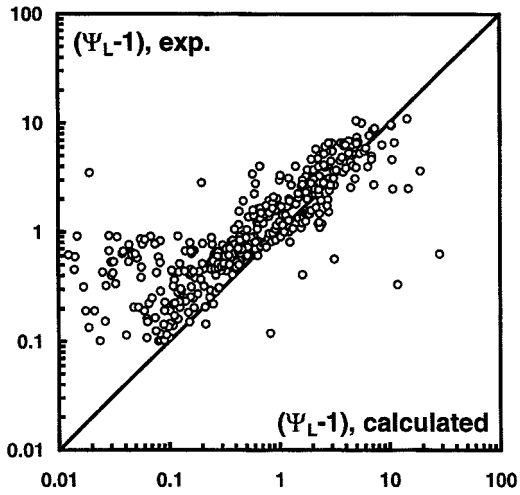

Figure 3. Holub shearless model predictions vs. dimensionless two-phase pressure-drop data for trickle-flow regime and partial wetting conditions over the whole database.

$f_v = 0$, $f_s = 0$, $\eta_e = 1.0$ (Holub et al., 1992, 1993).

Initial guesses for the liquid holdup and the pressure drop were made by the shearless Holub model ($\eta_e = 1$; Holub et al., 1992, 1993), whereas the wetting efficiency was initialized by putting $\Psi_L = 1$, $f_s = 0$ in Eq. 38 (free-falling liquid film and stagnant gas phase).

The pressure-drop parity plots of Figures 3 and 4 outline the inability of the shearless Holub model ($\eta_e = 1$, $f_s = 0$, $f_v = 0$; Holub et al., 1992, 1993) to predict adequately all of the frictional pressure-gradient data obtained through measurements taken for partially wetted beds in the trickle-flow regime using the elaborated database. As can be seen from the parity plot illustrated by Figure 4, a better fit on the pressure drops is attained when the present double-slit model, accounting for partial wetting, is coupled with the shear and slip velocity ANN correlations developed in this work. The respective scatters between the experimental data and the model predictions of the pressure drop and the liquid holdup are summarized in Table 8. Also included is a comparison of the extended Holub model (Iliuta et al., 1998), the "permeability" model (Saez and Carbonell, 1985), and the CFD model (Attou et al., 1999) performances. In all cases, the double-slit model outperformed all the available models in terms of the pressure-drop predictability. The relevance of the double-slit model ($f_s < 0$, $f_v < 0$, $\eta_e < 1$) over the extended Holub model

Table 7. Fitting Parameters of the Neural Network Correlation for the Velocity Slip Factor, f_v ($I = 6$, $J = 7$)

ω_{ij2}	1	2	3	4	5	6	7
1	−11.8606	22.3809	34.6526	60.7039	−23.7179	39.2532	43.0282
2	2.1394	8.7354	−31.6759	70.5865	−59.2732	−41.7112	−8.9428
3	6.3392	−21.4940	8.06859	−17.7233	−40.8304	7.9746	−43.5496
4	17.0921	−5.8241	29.9708	−35.9454	31.8167	17.3585	−33.3915
5	26.4843	11.5562	40.8534	−78.1653	12.4212	43.7787	19.1926
6	10.9552	17.5525	−2.8492	−54.6258	28.1273	−19.1004	−80.4211
7	3.0121	−20.0247	30.7862	54.1784	52.9346	16.6740	4.7819

ω_{j2}	1	2	3	4	5	6	7	8
	−14.7101	29.7982	34.4147	0.8863	1.0522	21.2524	4.2179	−42.0172

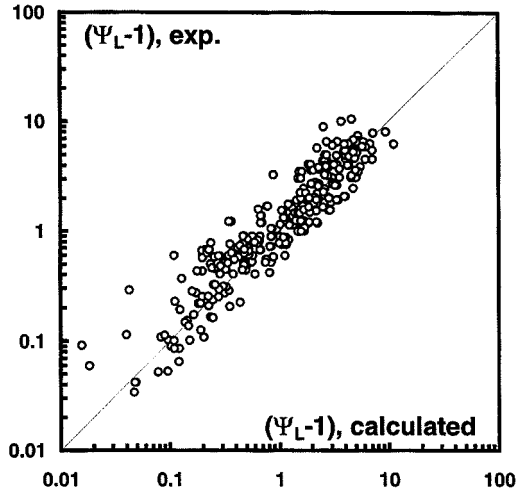

Figure 4. Double-slit model predictions vs. dimensionless two-phase pressure-drop data for trickle-flow regime and partial wetting conditions over the whole database.

$f_s \neq 0$, $f_v \neq 0$, $\eta_e < 1$.

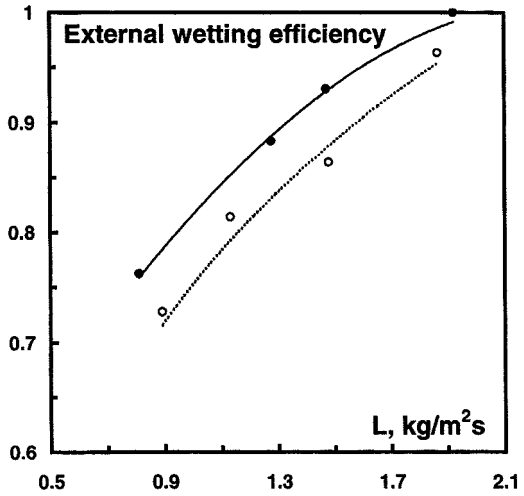

Figure 5. Effect of liquid mass velocity and reactor pressure on wetting efficiency.

System hexane–nitrogen, porous sphere, $d_p = 0.00152$ m, $d_c/d_p = 14.6$, $\epsilon = 0.412$, $v_{SG} = 0.085$ m/s; experimental, (○) $P = 0.31$ MPa, (●) $P = 3.55$ MPa (Al-Dahhan and Dudukovic, 1995); (——) double-slit model.

($f_s < 0$, $f_v < 0$, $\eta_e = 1$; Iluita et al., 1998) is demonstrated by the better pressure-drop predictions (Table 8). This observation suggests that the friction contribution over the dry surface to the overall pressure drop is physically well accounted for in the present model. The CFD model of Attou et al. (1999) gives better predictions for the pressure drop than the shearless Holub (1992) model. However, it remains less accurate than the other tested models regardless of the assumption of compressible (full model, 4 ODEs) or incompressible (simplified model, 2 ODEs) flow. The shearless Holub et al. (1992) model, although the differences are not very significant, offers a small advantage, leading the other models in terms of the liquid holdup predictions (see Table 8). In accordance with the earlier observations of Al-Dahhan et al. (1998), the Holub's model does not require precise correlations for f_s and f_v to forecast correctly liquid holdups. All five models, the double-slit model included, perform equally well and can be recommended indistinguishably in liquid holdup predictions. However, except the double-slit model, the inherent limitation of the other models lies in their inability to predict the wetting efficiency.

Table 8. Prediction Capabilities of Current Trickle Flow Models

	Statistical Parameter					
	AARE (%)			σ (%)		
Reference	Ψ_L	ϵ_L	η_e	Ψ_L	ϵ_L	η_e
Saez and Carbonell (1985)	46	26	—	26	82	—
Holub et al. (1992)	69	21	—	25	19	—
Extended Holub model*	41	25	—	22	16	—
Attou et al. (1999)	58**	23**	—	48	17	—
	57†	25†	—	46	31	—
Pironti et al. (1999)††	—	—	> 100	—	—	—
Double-slit model‡	32	24	8	23	29	10

*Iliuta et al. (1998).
**Simplified model (2 ODEs): neglecting compressibility effects.
†Original model (4 ODEs): accounting for compressibility effects.
††Diverged for high-pressure drop data of Al-Dahhan and Dudukovic data (1995, 1996).
‡Using all tested wetting efficiency data of this work.

External wetting efficiency

The wetting efficiency data used for model validation comes from tests related to spherical and nonspherical monodisperse catalyst particles, mixtures of fines with catalyst particles, elevated pressure ($0.31 \leq P \leq 10$ MPa; Ring and Missen, 1991; Al-Dahhan and Dudukovic, 1995, 1996) and high temperature (573–623 K; Ring and Missen, 1991; Llano et al., 1997). Figure 5 shows that the developed model predicts well the trend of reactor pressure and liquid flow rate effects on the wetting efficiency (data of Al-Dahhan and Dudukovic, 1995). As the pressure drop increases at fixed liquid velocity due to higher reactor pressure, both the liquid holdup and the liquid-film thickness decrease (results not shown here). This increase in the pressure drop increases the shear stress on the gas–liquid interface, that is, via f_s and f_v, and results in an improved spreading of the liquid film over the external packing area making it more wet (Al-Dahhan and Dudukovic, 1996). As the liquid flow rate increases, both the liquid holdup and the pressure drop increase, thus yielding to a further improvement in the wetting efficiency. Figure 6 is a parity plot showing the measured wetting efficiency data, η_e, vs. the predicted ones using Eqs. 20, 21 and 38 (data of Ring and Missen, 1991; Al-Dahhan and Dudukovic, 1995, 1996: Llano et al., 1997). The model successfully predicts the wetting efficiency at high temperature (AARE = 15%), high pressure (AARE = 10%), as well as for diluted-bed conditions (AARE = 3%) (see also Table 8 for a performance comparison with the Pironti et al. (1999) wetting efficiency model). Laboratory-scale TBRs consisting of mixtures of fines and catalyst pellets of the same shape and size as in commer-

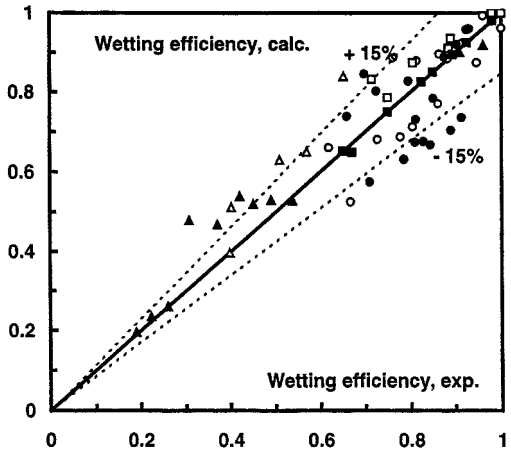

Figure 6. Predicted vs. experimental wetting efficiency.

(○)—spherical particles; (●)—cylindrical particles (Al-Dahhan and Dudukovic, 1995); (□)—spherical particles with fines; (■)—cylindrical particles with fines (Al-Dahhan and Dudukovic, 1996); (△)—spherical particles (Ring and Missen, 1991); (▲)—spherical particles (Llano et al., 1997).

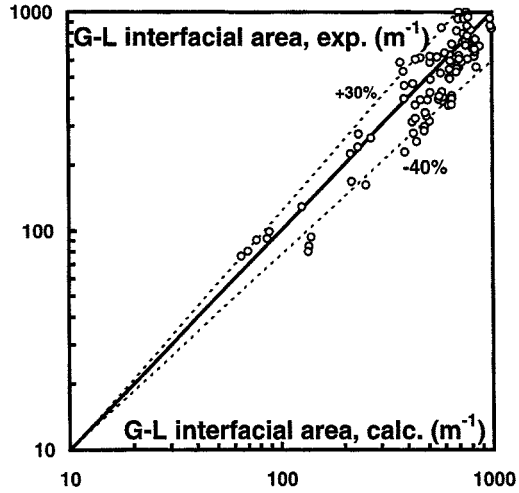

Figure 7. Parity plot for the prediction of the gas–liquid interfacial area in trickle-flow regime using the double-slit model.

cial-scale TBRs are used as a small-scale replica to mimic, in the catalytic reaction sense, the commercial-size reactor performances (Al-Dahhan and Dudukovic, 1996). Therefore these results relative to laboratory-scale beds diluted with fines and operated at high pressure and temperature are of industrial relevance, since it is now possible to tailor in advance the bed composition for scale-down and for achieving a desired wetting quality of catalysts.

Moreover, as the present hybrid approach retains many of the advantages of the phenomenological character of the double-slit model, it also is expected to provide meaningful simulations of the hydrodynamics for scale-up, scale-down, and design of commercial trickle-flow reactors. In practice for *scale-down purposes*, the model can be particularly useful at predicting the wetting efficiency to be achieved in pilot- or lab-scale reactors, for given catalyst/feed stocks, to match the liquid hour space velocity (LHSV) of a large-scale trickle-flow reactor where usually high liquid throughputs are fed to ensure full wetting of the catalyst pellets in the case of liquid-limited reactions.

Gas–liquid interfacial area

The experimental conditions, under which the gas–liquid interfacial area can be predicted by the double-slit model from the dynamic external wetting efficiency and the bed-specific surface area, will be delineated. Figure 7 compares the gas–liquid interfacial areas predicted values (Eq. 41) with the corresponding interfacial area data from the database described in Table 4. The agreement between the proposed model predictions and the experimental data is satisfactory for the high-pressure mass-transfer data and for the atmospheric measurements only at moderately high gas superficial velocities ($v_{SG} > 0.2$ m/s). A plausible physical interpretation to this observation is that high pressure and/or high gas flow rates promote the pressure drop, thereby enhancing the gas–liquid shear stress with, as a result, an improved spreading of the liquid film over the external packing area. In these conditions the liquid film thickness gets more uniform and the packing area wetting by the dynamic liquid holdup (or the dynamic wetting efficiency) approximates very well the gas–liquid interfacial area. At the low gas superficial velocities and close to the atmospheric pressure, the double-slit model tended to overestimate the gas–liquid interfacial area. This could be explained from the fact that due to the weak gas momentum, the gas flow cannot penetrate or break the liquid structures such as liquid bridges surrounding clusters of particles in the porous medium. These bridges are likely to imprison gas pockets in the form of static gas holdup. Such gas pockets are ineffective in the gas–liquid mass-transfer sense and are consequently invisible to the chemical absorption techniques that served to measure the effective gas–liquid interfacial area. Nevertheless, this limitation is not an obstacle, since the majority of commercial-scale trickle-flow reactors operate at high pressure, and therefore the double-slit model can be effectively used to make gas–liquid interfacial area predictions under those conditions.

The two available correlations relative to the gas–liquid interfacial area prediction validated over wide-ranging operating conditions are summarized in Table 2. The results of the average absolute relative error, obtained by comparing the performance of these correlations and the double-slit model using a set of data contained in the collected database, are presented in Table 9. The Wild et al. (1992) trickle-flow correlation exhibits an excessively high error and appears to be inadequate in predicting the partial wetting conditions deep in the trickle-flow regime. The double-slit model predicts the interfacial area equally well as the Iliuta et al. (1999) neural

Table 9. Predictions of Interfacial Area in Trickle Flow by Current Tools

Reference	AARE (%)
Wild et al. (1992)	118
Iliuta et al. (1999)	29
Double-slit model	32

network (empirical) correlation developed from the same data as those used in the present study.

Summary and Concluding Remarks

An implicit semitheoretical mechanistic two-fluid double-slit model was indeed developed for the prediction of the frictional two-phase pressure drop, the liquid holdup, the external wetting efficiency, and the gas–liquid interfacial area in trickle-flow reactors operated under partially wetted conditions. The model is an extension of the Holub phenomenological shearless model. It incorporates both the partial wetting conditions at the pellet scale and the improved slip factor correlations to account for the shear-stresses contribution at the dry pellet–gas and the gas–liquid interfaces to the overall frictional pressure gradient. The bed geometry and two-phase flow were mapped to a representative pellet-scale recurrent unit cell of two parallel interconnected inclined slits, that is, ''the double-slit.''

The two-phase flow is decomposed into three streams (2 for the gas and 1 for the liquid). The wet slit is crossed by the liquid stream and one of the gas streams, and the dry slit is traversed by the second gas stream only. The model requires the bed Ergun constants, the static liquid holdup, and the shear and velocity slip factors to be evaluated prior to its use. In particular two efficient slip factor correlations relying on artificial neural networks, dimensional analysis, and a wide historic trickle-flow database were established for the description of shear and velocity slip in the partially wetted trickle-flow regime. The double-slit model outperformed other available models in the prediction of the pressure drop and the liquid holdup data related to partial wetting conditions. The pressure drop and the liquid holdup were predicted with average relative errors estimated, respectively, at 32% and 24%. These errors reflect (1) the erratic behavior of the two-phase texture deep in the trickle-flow regime and partially wetted porous media, (2) the higher sensitivity of fluid distribution to bed and to distributor imperfections, and (3) the difficulty to measure hydrodynamic parameters with high accuracy, as for instance in the pulse-flow regime.

The wetting efficiency model is the first quantitative phenomenological formulation of the relationship between the wetting efficiency, the pressure drop, and the liquid holdup in the trickle-flow regime. The model can predict the transition between partial wetting and full wetting of the bed pellets. High-pressure and high-temperature wetting efficiency data as well as data measured in beds made up of mixtures of commercial-size catalyst particles and fines were also well predicted. The prediction error introduced by the model was always better than 15%. The model is particularly useful (1) for iso-LHSV *scale-down* of ''liquid-limited'' processes, (2) for disentangling chemical kinetics from hydrodynamic effects by assessing the wetting extent in lab-scale fine-catalyst mixed-bed replica, and (3) for *scale-up* and design of industrial reactors by characterizing the *minimum* required gas and liquid throughputs to ensure full wetting of the catalyst pellets.

Assuming a structural relationship between the dynamic wetting efficiency, the total wetting efficiency, the static liquid holdup, and the gas–liquid interfacial area, the double-slit model was extended to estimate with acceptable accuracy the gas–liquid interfacial areas in the trickle-flow regime. The model surpasses all available mass-transfer correlations with the exception of the recent Iliuta et al. (1999) correlation elaborated using the same database.

The advantage of the double-slit model to describe simultaneously several hydrodynamic and mass-transfer parameters in the trickle-flow regime makes it an attractive model for two reasons: (1) traditionally the pressure drop, the liquid holdup, the wetting efficiency, the interfacial area, and the full-to-partial wetting boundary are obtained using as many correlations having different accuracy and usually derived on narrow-ranging experimental intervals, and (2) the database that served for the test of the double-slit model is the widest ever built for the partial-wetting trickle-flow conditions. The benefit of this model is that it provides a unique framework expressing quantitatively the interconnection between pressure drop, liquid holdup, wetting efficiency, and gas–liquid interfacial area, and which is validated upon the widest trickle-flow hydrodynamic database ever built. It is hoped that this will move the trickle-bed design approaches away from using a mixed bag of correlations developed from limited data toward an experimental program having more fundamental bases.

Acknowledgments

Financial support from the National Sciences and Engineering Research Council of Canada and the Fonds pour la Formation de Chercheurs et l'Aide à la Recherche du Québec is gratefully acknowledged.

Notation

a = gas–liquid interfacial area, m^2/m^3
a_s = packing-specific area (surface of particles/bed volume), m^2/m^3
d_c = column diameter, m
d_h = Krischer and Kast hydraulic diameter, $d_h = d_p\sqrt[3]{16\epsilon^3/9\pi(1-\epsilon)^2}$, m
d_p = equivalent diameter based on a sphere of equal volume, m
Eo = Eötvös number, $Eo = d_p^2 g \rho_L/\sigma_L$
Eo_m = modified Eötvös number, $Eo_m = \rho_L g d_p^2 \phi^2 \epsilon^2/\sigma_L(1-\epsilon)^2$
Fr_L = liquid Froude number, $Fr_L = v_{SL}^2/gd_p$
g = gravity acceleration, m/s^2
Ga = Galileo number, $Ga = d_p^3 g \rho_L^2/\eta_L^2$
Ga_α = bed Galileo number, $Ga_\alpha = d_p^3 g \epsilon^3/[\nu_\alpha^2(1-\epsilon)^3]$
H = hidden-layer vector
K = number of output nodes
L = liquid flow rate, $kg/m^2 s$
N = number of data
P = pressure, Pa
$\Delta P/H$ = two-phase frictional pressure drop, Pa/m
Re_i = interfacial Reynolds number
Re_α = Reynolds number, $Re_\alpha = v_{S\alpha} d_p/[\nu_\alpha(1-\epsilon)]$
S_b = bed correction function, $S_b = a_s d_h/(1-\epsilon)$
S_D = half-wall thickness, m
u_α = velocity of α phase in the slit, m/s
$u_{i\alpha}$ = interfacial velocity of α phase, m/s
U_i = normalized input variables
w = half void thickness in the slit model, m
We_L = liquid Weber number, $We_L = v_{SL}^2 d_p \rho_L/\sigma_L$
x = coordinate in a plan normal to z, m
y = hydrodynamic parameter ($y = \epsilon_L$, $\Delta P/H$, a, η_e)
α = meaning gas (G) or liquid (L)
β_L = liquid saturation
δ = liquid-film thickness, m
ϵ = bed porosity
ϵ_α = holdup of α phase
ϕ = sphericity factor

μ_α = viscosity of α phase, kg/m·s
η_e = external wetting efficiency
λ = slip parameter in Attou et al. (1999) model, $\lambda = 1-(v_{sL}/v_{sG})[\epsilon_L/(\epsilon-\epsilon_L)]$
ν_α = kinematic viscosity of α phase, m^2/s
ρ_α = density of α phase, kg/m^3
σ = standard deviation

$$\sqrt{\frac{\sum_{i=1}^{N}\left[\left|\frac{y_{\text{calc},i}-y_{\text{exp},i}}{y_{\text{exp},i}}\right|-\text{AARE}\right]^2}{N-1}}$$

σ_L = surface tension, N/m

Subscripts

a = acceleration/deceleration
calc = calculated
d = dynamic
exp = experimental
g = gravitational
G = gas
L = liquid
st = static
t = total

Literature Cited

Al-Dahhan, M. H., "Effects of High Pressure and Fines on the Hydrodynamics of Trickle-Bed Reactors," DSc Thesis, Washington Univ., St. Louis, MO (1993).

Al-Dahhan, M. H., and M. P. Dudukovic, "Catalyst Wetting Efficiency in Trickle-Bed Reactors at High Pressure," *Chem. Eng. Sci.*, **50**, 2377 (1995).

Al-Dahhan, M. H., and M. P. Dudukovic, "Catalyst Bed Dilution for Improving Catalyst Wetting in Laboratory Trickle-Bed Reactors," *AIChE J.*, **42**, 2594 (1996).

Al-Dahhan, M. H., M. R. Khadilkar, Y. Wu, and M. P. Dudukovic, "Prediction of Pressure Drop and Liquid Hold-Up in High-Pressure Trickle-Bed Reactors," *Ind. Eng. Chem. Res.*, **37**, 793 (1998).

Alicilar, A., A. Bicer, and A. Murathan, "The Relation Between Wetting Efficiency and Liquid Hold-Up in Packed Columns," *Chem. Eng. Commun.*, **128**, 95 (1994).

Attou, A., C. Boyer, and G. Ferschneider, "Modelling of the Hydrodynamics of the Cocurrent Gas-Liquid Trickle-Flow Through a Trickle-Bed Reactor," *Chem. Eng. Sci.*, **54**, 785 (1999).

Azzaz, M. S., "Réacteurs Gaz-Liquide-Solide à Lit Fixe: Réactions Catalytiques, Hydrodynamique et Transfert de Matière," PhD Thesis, Institut National Polytechnique de Lorraine, Nancy, France (1984).

Bakos, M., P. Arva, and F. Szeifert, "Interfacial Area in Packed Bed Gas-Liquid Reactors with Co-Current Downward Flow," *Hung. J. Ind. Chem.*, **8**, 383 (1980).

Brunazzi, E., and A. Paglianti, "Mechanistic Pressure Drop Model for Columns Containing Structured Packings," *AIChE J.*, **43**, 317 (1997).

Burghardt, A., G. Bartelmus, M. Jaroszynski, and A. Kolodziej, "Hydrodynamics and Mass Transfer in a Three-Phase Fixed-Bed Reactor with Cocurrent Gas-Liquid Downflow," *Chem. Eng. J.*, **58**, 83 (1995).

Charpentier, J. C., "Hydrodynamique des Colonnes à Garnissage avec Écoulement de Gaz et de Liquide à Co-Courant et à Contre-Courant. Aspects Statique et Dynamique de la Texture du Liquide," PhD Thesis, Univ. of Nancy, Nancy, France (1968).

Cloutier, P., C. Tibirna, B. P. A. Grandjean, and J. Thibault, "NNFit Logiciel de Régression Utilisant les Réseaux à Couches," http://www.gch.ulaval.ca/~nnfit (1996).

Dudukovic, M. P., "Catalyst Effectiveness Factor and Contacting Efficiency in Trickle-Bed Reactors," *AIChE J.*, **23**, 6 (1977).

Dudukovic, M. P., and P. L. Mills, "Contacting and Hydrodynamics in Trickle-Bed Reactors," *Encyclopedia of Fluid Mechanics*, Chap. 32, N. P. Cheremisinoff, ed., Gulf Pub., Houston, p. 969 (1986).

Dudukovic, M. P., F. Larachi, and P. L. Mills, "Multiphase Reactors—Revisited," *Chem. Eng. Sci.*, **54**, 1975 (1999).

El-Hisnawi, A. A., "Tracer and Reaction Studies in Trickle-Bed Reactors," DSc Thesis, Washington Univ., St. Louis, MO (1981).

Fukushima, S., and K. Kusaka, "Interfacial Area and Boundary of Hydrodynamic Flow Region in Packed Column with Cocurrent Downward Flow," *J. Chem. Eng. Jpn.*, **10**, 461 (1977a).

Fukushima, S., and K. Kusaka, "Liquid-Phase Volumetric and Mass Transfer Coefficient, and Boundary of Hydrodynamic Flow Region in Packed Column with Cocurrent Downward Flow," *J. Chem. Eng. Jpn.*, **10**, 468 (1977b).

Holub, R. A., "Hydrodynamics of Trickle Bed Reactors," DSc Thesis, Washington Univ., St. Louis, MO (1990).

Holub, R. A., M. P. Dudukovic, and P. A. Ramachandran, "A Phenomenological Model for Pressure Drop, Liquid Hold-Up, and Flow Regime Transition in Gas-Liquid Trickle Flow," *Chem. Eng. Sci.*, **47**, 2343 (1992).

Holub, R. A., M. P. Dudukovic, and P. A. Ramachandran, "Pressure Drop, Liquid Hold-Up and Flow Regime Transition in Trickle Flow," *AIChE J.*, **39**, 302 (1993).

Iliuta, I., "Hydrodynamics and Mass Transfer in Multiphase Fixed Bed Reactors," PhD Thesis, Univ. Catholique de Louvain, Louvain, Belgium (1996).

Iliuta, I., F. C. Thyrion, and O. Muntean, "Hydrodynamic Characteristics of Two-Phase Flow Through Fixed Beds: Air/Newtonian and Non-Newtonian Liquids," *Chem. Eng. Sci.*, **51**, 4987 (1996).

Iliuta, I., F. Larachi, and B. P. A. Grandjean, "Pressure Drop and Liquid Hold-Up in Trickle Flow Reactors: Improved Ergun Constants and Slip Correlations for the Slit Model," *Ind. Eng. Chem. Res.*, **37**, 4542 (1998).

Iliuta, I., F. Larachi, B. P. A. Grandjean, and G. Wild, "Gas-Liquid Interfacial Mass Transfer in Trickle-Bed Reactors: State-of-the-Art-Correlations," *Chem. Eng. Sci.*, **54**, 5633 (1999).

Krauze, R., and M. Serwinski, "Moisted Surface and Fractional Wetted Area of Ceramic Raschig Rings," *Inzineria Chem.*, **1**, 415 (1971).

Lakota, A., "Hydrodynamics and Mass Transfer Characteristics of Trickle-Bed Reactors," PhD Thesis, Univ. of Ljubljana, Ljubljana, Slovenia (1990).

Lakota, A., and J. Levec, "Solid-Liquid Mass Transfer in Packed Beds with Cocurrent Downward Two-Phase Flow," *AIChE J.*, **36**, 1444 (1990).

Larachi, F., "Les Réacteurs Triphasiques à Lit Fixe à Écoulement à Co-Courant Vers le Bas et Vers le Haut de Gaz et de Liquide. Étude de l'Influence de la Pression sur l'Hydrodynamique et le Transfert de Matière Gaz-Liquide," PhD Thesis, Institut National Polytechnique de Lorraine, Nancy, France (1991).

Larachi, F., A. Laurent, G. Wild, and N. Midoux, "Some Experimental Liquid Saturation Results in Fixed-Bed Reactors Operated Under Elevated Pressure in Cocurrent Upflow and Downflow of the Gas and the Liquid," *Ind. Eng. Chem. Res.*, **30**, 2404 (1991a).

Larachi, F., A. Laurent, N. Midoux, and G. Wild, "Experimental Study of a Trickle-Bed Reactor Operating at High Pressure: Two-Phase Pressure Drop and Liquid Saturation," *Chem. Eng. Sci.*, **46**, 1233 (1991b).

Larachi, F., A. Laurent, G. Wild, and N. Midoux, "Pressure Effects on Gas-Liquid Interfacial Area in Cocurrent Trickle-Flow Reactors," *Chem. Eng. Sci.*, **47**, 2325 (1992).

Larachi, F., M. Cassanello, A. Laurent, N. Midoux, and G. Wild, "Gas-Liquid Interfacial Areas in Three-Phase Fixed Bed Reactors," *Chem. Eng. Process*, **36**, 497 (1997).

Larachi, F., M. Cassanello, and A. Laurent, "Gas-Liquid Interfacial Mass Transfer in Trickle-Bed Reactors at Elevated Pressures," *Ind. Eng. Chem. Res.*, **37**, 718 (1998).

Latifi, M. A., A. Naderifar, and N. Midoux, "Energetic Analysis of the Liquid-to-Wall Mass Transfer in a Trickle-Bed Reactor," *Trans. Inst. Chem. Eng.*, **77**, 69 (1999).

Lazzaronni, C. L., H. R. Keselman, and H. S. Figoli, "Colorimetric Evaluation of the Efficiency of Liquid-Solid Contacting in Trickle-Flow," *Ind. Eng. Chem. Res.*, **27**, 1132 (1988).

Llano, J. J., R. Rosal, H. Sastre, and F. Diez, "Determination of Wetting Efficiency in Trickle-Bed Reactors by a Reaction Method," *Ind. Eng. Chem. Res.*, **36**, 2616 (1997).

Mahajani, V. V., and M. M. Sharma, "Effective Interfacial Area and Liquid Side Mass Transfer Coefficient in Trickle Bed Reactors," *Chem. Eng. Sci.*, **34**, 1425 (1979).

Mahajani, V. V., and M. M. Sharma, "Mass Transfer in Packed

Columns: Cocurrent (Downflow) Operation: 1 in. and 1.5 in. Metal Pall Rings and Ceramic Intalox Saddles: Multi-Filament Gauze Packings in 20 cm and 38 cm I.D. Columns,'' *Chem. Eng. Sci.*, **35**, 941 (1980).

McManus, R. L., G. A. Funk, M. P. Harold, and K. M. Ng, ''Experimental Study of Reaction in Trickle-Bed Reactors with Liquid Maldistribution,'' *Ind. Eng. Chem. Res.*, **32**, 570 (1993).

Meyers, R. A., *Handbook of Petroleum Refining Processes*, 2nd ed., McGraw-Hill, New York (1996).

Mills, P. L., and M. P. Dudukovic, ''Evaluation of Liquid-Solid Contacting in Trickle Beds by Tracer Methods,'' *AIChE J.*, **27**, 893 (1981).

Mills, P. L., and M. P. Dudukovic, ''Integral Equation Solution for the Effectiveness Factor of Partially Wetted Catalysts,'' *Ind. Eng. Chem.*, **21**, 1 (1982).

Morsi, B. I., N. Midoux, and J. C. Charpentier, ''Flow Patterns and Some Hold-Up Experimental Data in Trickle-Bed Reactors for Foaming, Nonfoaming, and Viscous Organic Liquids,'' *AIChE J.*, **24**, 357 (1978).

Morsi, B. I., ''Hydrodynamique, Aires Interfaciales et Coefficients de Transfert de Matière Gaz-Liquide dans les Réacteurs Catalytiques à Lit Fixe Arrosé: Les Résultats Obtenus en Milieu Liquide Aqueux Académique Sont-Ils Encore Représentatifs en Milieu Organique Industriel?,'' PhD Thesis, Institut National Polytechnique de Lorraine, Nancy, France (1982).

Morsi, B. I., N. Midoux, A. Laurent, and J. C. Charpentier, ''Hydrodynamics and Interfacial Areas in Downward Cocurrent Gas-Liquid Flow through Fixed Beds. Influence of the Nature of the Liquid,'' *Int. Chem. Eng.*, **22**, 142 (1982).

Morsi, B. I., A. Laurent, N. Midoux, G. Barthole-Delanauy, A. Storck, and J. C. Charpentier, ''Hydrodynamics and Gas-Liquid-Solid Interfacial Parameters of Co-Current Downward Two-Phase Flow in Trickle-Bed Reactors,'' *Chem. Eng. Commun.*, **25**, 267 (1984).

Onda, K., H. Takeuchi, and Y. Kayama, ''Effect of Packing Materials on Wetted Surface Area,'' *Kagaku Kogaku*, **31**, 126 (1967).

Pironti, F., D. Mizrahi, A. Acosta, and D. Gonzalez-Mendizibal, ''Liquid-Solid Wetting Factor in Trickle-Bed Reactors: Its Determination by a Physical Method,'' *Chem. Eng. Sci.*, **54**, 3793 (1999).

Puranik, S. S., and V. Vogelpohl, ''Effective Interfacial Area Irrigated Packed Columns,'' *Chem. Eng. Sci.*, **29**, 501 (1974).

Rajashekharam, M. V., R. Jaganathan, and R. V. Chaudhari, ''A Trickle-Bed Reactor Model for Hydrogenation of 2,4 Dinitrotoluene: Experimental Verification,'' *Chem. Eng. Sci.*, **53**, 787 (1998).

Ratnam, V. G. S., V. D. Narasaiah, and Y. B. G. Varma, ''A Correlation for Interfacial Area in Cocurrent Gas-Liquid Downflow Through Packed Beds,'' *Bioprocess Eng.*, **10**, 53 (1994).

Ring, Z. E., and R. W. Missen, ''Trickle-Bed Reactors: Tracer Study of Liquid Hold-Up and Wetting Efficiency at High Temperature and Pressure,'' *Can. J. Chem. Eng.*, **69**, 1016 (1991).

Ruecker, C. M., and A. Akgerman, ''Determination of Wetting Efficiencies for a Trickle-Bed Reactor at High Temperature and Pressure,'' *Ind. Eng. Chem. Res.*, **26**, 164 (1987).

Saez, A. E., and R. G. Carbonell, ''Hydrodynamic Parameters for Gas-Liquid Cocurrent Flow in Packed Beds,'' *AIChE J.*, **31**, 52 (1985).

Shende, B. W., and M. M. Sharma, ''Mass Transfer in Packed Columns: Cocurrent Operation,'' *Chem. Eng. Sci.*, **29**, 1763 (1974).

Shulman, H. L., C. F. Ullrich, A. Z. Proulx, and J. O. Zimmerman, ''Performance of Packed Column II: Wetted and Effective Interfacial Area, Gas and Liquid Mass Transfer Rates,'' *AIChE J.*, **1**, 253 (1955).

Toye, D., P. Marchot, M. Crine, and G. L'Homme, ''Computer-Assisted Tomography for Liquid Imaging in Trickle Flow Columns,'' *Non-Invasive Monitoring of Multiphase Flows*, Chap. 3, J. Chaouki, F. Larachi, and M. P. Dudukovic, eds., Elsevier, The Netherlands, p. 105 (1997).

Wammes, W. J. A., ''Hydrodynamics in a Cocurrent Gas-Liquid Trickle-Bed Reactor at Elevated Pressures,'' PhD Thesis, Twente Univ., Enschede, The Netherlands (1990).

Wammes, W. J. A., J. Middelkamp, W. J. Huisman, C. M. de Baas, and K. R. Westerterp, ''Hydrodynamics in a Cocurrent Gas-Liquid Trickle Bed at Elevated Pressures, Part 1: Gas-Liquid Interfacial Areas, Part 2: Liquid Hold-Up, Pressure Drop, Flow Regimes,'' *AIChE J.*, **37**, 1849 (1991a).

Wammes, W. J. A., S. J. Mechielsen, and K. R. Westerterp, ''The Influence of Pressure on the Liquid Hold-Up in a Concurrent Gas-Liquid Trickle-Bed Reactor Operating at Low Gas Velocities,'' *Chem. Eng. Sci.*, **46**, 409 (1991b).

Wild, G., F. Larachi, and J. C. Charpentier, ''Heat and Mass Transfer in Gas-Liquid-Solid Fixed Bed Reactors,'' *Heat and Mass Transfer in Porous Media*, M. Quintard and M. Todorovic, eds., Elsevier, Amsterdam, The Netherlands, p. 616 (1992).

Yaïci, W., ''Mise au Point de Nouveaux Systèmes d'Absorption Gaz-Liquide avec Réaction Chimique en Milieux Liquides Aqueux et Organique en Vue de Leur Application à la Détermination par Méthode Chimique de la Conductance de Transfert de Matière en Phase Gazeuse dans un Réacteur Catalytique à Lit Fixe Arrosé,'' PhD Thesis, Institut National Polytechnique de Lorraine, Nancy, France (1985).

Yaïci, W., A. Laurent, N. Midoux, and J. C. Charpentier, ''Détermination des Coefficients de Transfert de Matière en Phase Gazeuse dans un Réacteur Catalytique à Lit Fixe Arrosé en Présence de Phases Liquides Aqueuses et Organiques,'' *Bull. Soc. Chim. France*, **6**, 1032 (1985).

Yaïci, W., A. Laurent, N. Midoux, and J. C. Charpentier, ''Determination of Gas-Side Mass Transfer Coefficients in Trickle-Bed Reactors in the Presence of an Aqueous or an Organic Liquid Phase,'' *Int. Chem. Eng.*, **28**, 299 (1988).

Zhukova, T., B. V. N. Pisarenko, and V. V. Kafarov, ''Modeling and Design of Industrial Reactors with a Stationary Bed of Catalyst and Two-Phase Gas-Liquid Flow—A Review,'' *Int. Chem. Eng.*, **30**, 57 (1990).

Manuscript received May 26, 1999, and revision received Oct. 14, 1999.